Blind source separation in the physical layer

Alexander N. Tait*, Thomas Ferreira de Lima*, Philip Y. Ma*, Matthew P. Chang*,†,
Mitchell A. Nahmias*, Bhavin J. Shastri*, Prateek Mittal*, and Paul R. Prucnal*
* Princeton University, Princeton, NJ 08540   † Apple Inc., Cupertino, CA 95014
atait@princeton.edu

Abstract—**Multi-antenna radio systems exploit spatial inhomogeneity to share wireless resources. Blind source separation is a powerful capability that can reduce many received signals into a salient estimate of independent transmitters. Performing blind source separation in the analog, physical layer promises significant performance improvements but presents a problem in that not all received signals can be observed at the same time. We propose a novel algorithm that synthesizes univariate statistics to reconstruct the multivariate statistical properties required for blind source separation. Using analog photonic hardware, we demonstrate experimental techniques for obtaining the required information while remaining true to realistic constraints on observability. Finally, we provide an example application for using the physical layer to preserve privacy in spectrum monitoring operations. The concepts and techniques developed lay a groundwork for further research in blind multivariate analysis in the high-performance analog domain.**

I. Introduction

The accelerating demands on wireless resources are pushing radio operations towards new regimes of performance and new modalidies of access [1], [2]. Multi-antenna systems exploit spatial inhomogeneity in the electromagnetic field, promising a new degree of freedom with which to share wireless resources [3]. Signals received by different antennas are typically highly correlated. These redundant, high-dimensional signals are projected into a salient, few-dimensional representation. Weighted addition (i.e. vector dot product) is the elemental multi-input, single-output function underlying dimensionality reduction. A key challenge is determining the weight vectors that produce a salient output.

Principal component analysis (PCA) and independent component analysis (ICA) are eminent strategies for reducing correlated multivariate signals to more salient signals [4]. Each output, called a principal/independent component (PC/IC), is a linear projection of the original inputs onto a corresponding principal/independent component vector (PC/IC vector). PCA yields decorrelated output signals, sorted in descending order of statistical relevance. The highest PCs can be discarded to reduce overall dimensionality while losing the minimum salient overall information.

ICA is more useful in the RF context because it separates independent signals corresponding to multiple source transmitters that have been mixed over a wireless channel. The problem of blind source separation (BSS) is tremendously useful and widely applicable in radio and has been studied extensively using digital signal processing [5]. ICA employs the central limit theorem, which states that the statistical distribution of multiple independent random variables is always more Gaussian that those of the originals. Gaussianity is measured by the 4th-order moment (a.k.a. kurtosis), which is 3 for an ideal Gaussian. The ICs are thus the vectors that maximize the relative kurtosis. Normally, radio sources are separated based on a priori knowledge of their characteristics. For example, sources of different and known center frequencies can be separated by a filter, and sources of differnt and known arrival angles can be separated by a phased-array antenna. In constrast, BSS assumes no a priori knowledge about the sources besides independence. In this paper, we constrain study to an instantaneous mixing channel, noting that approaches to multipath ICA could be explored in future work [6].

In the blind source separation problem, received signals, $\vec{x}$, are an unknown mixture, $\mathbf{A}$, of unknown source signals, $\vec{s}$: $\vec{x}(t) = \mathbf{A} \cdot \vec{s}(t)$. On the receiver front-end, there is a projection of these signals along the weight vector, $\vec{w}$ to produce the output m: $m(t) = \vec{w} \cdot \vec{x}(t)$. The goal of BSS is to find the independent component vectors, $\vec{w}_{IC,n}$, such that this output is an estimate of the original sources:

$$\hat{s}_n(t) = \vec{w}_{IC,n} \cdot \vec{x}(t) \quad \forall \ \ n \in \{1, \dots, N\} \qquad (1)$$

where $\hat{s}_n$ is the optimal estimate of the nth original source, and subscripts (IC, n) correspond to the independent components of the received signals.

In state-of-the-art digital signal processing (DSP), the IC vectors are estimated by examining the covariance and cokurtosis matrices of the received signals. Each antenna requires its own ADC, even though most of this digitized data is then discarded (Fig. 1a). ADC is a dominant power consumer because it's rate scales in proportion to the number of antennas and the sampling frequency [7], [8]. Performing dimensionality reduction in the analog domain can circumvent the ADC performance bottleneck. A single ADC digitizes only the demixed signal of interest. Hybrid analog-digital beamformers employing analog weighted addition have been explored [9]–[11] and were reviewed in Ref. [12]. Fig. 1b shows a photonic implementation of analog weighted addition. In this paper, we use RF photonic hardware to demonstrate key principles experimentally; however, the concepts and algorithms introduced here are applicable to other analog circuitry.

A. Hybrid channel estimation

Simultaneous samples of the received signals are typically required to perform PCA and ICA [13]; however, the
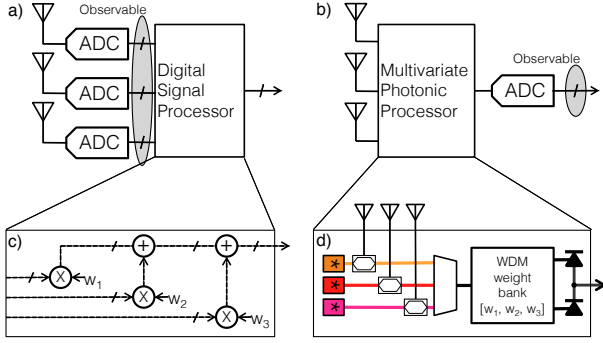
Fig. 1. Comparison of multi-antenna radio front-ends followed by dimensionality reduction. a) Dimensionality reduction with electronic DSP in which each antenna requires an ADC. b) Dimensionality reduction in the analog domain (a.k.a physical layer) in which only one ADC is required. A photonic implementation of weighted addition is pictured, consisting of electrooptic modulation, WDM filtering, and photodetection.

Fig. 2. Concept of building multivariate statistics based on observable univariate statistics for different covariance parameters, alpha. (Top) Black points: synchronously sampled 2-channel data plotted against one another. Synchronous samples are observed by conventional algorithms, but not observable after physcical layer dimensionality reduction. Black dashed curves: variance of the projected signal $\langle m^2 \rangle_t$ vs. projection angle θ. Colored lines: measurements of the projected signal variance for 5 angles. (Bottom) Histograms of the projected signal, $m = \vec{w} \cdot \vec{x}$, at the corresponding angles.

performance advantages of analog dimensionality reduction stem directly from *not* digitizing and observing all inputs. Ghauch et al. [14] offered a potent statement of the problem: "Channel estimation and precoding in hybrid analog-digital millimeter-wave (mmWave) MIMO systems is a fundamental problem that has yet to be addressed, before any of the promised gains can be harnessed." Recent strides have been made to address this problem in cooperative scenarios with bidirectional communication, typically referred to as MIMO [14]–[18]. Many of these approaches use training signals sent during an estimation phase (exception by Dahl et al. [18]) and/or a channel sparsity assumption (exception by Zanjani et al. [17]). Iltis et al. [19] studied a non-cooperative scenario using a game theoretic approach, which must assume that all transceivers abide by a common protocol.

II. THEORY

In contrast to prior work, we study the BSS scenario in which no a priori assumptions are made about transmitters' signal format, behavior, or cooperation. We propose an algorithm for identifying the ICs of an unknown mixture based only on the observations of a single projected output. The strategy is to reconstruct the multivariate statistics by synthesizing univariate statistics of the projected signal over multiple projection vectors. The significance of this algorithm is its compatibility with the constraints of analog and hybrid multi-antenna front-ends.

A. Projected moment information

At a given time, only one projection is observed digititally. When the projection vector is an IC, the output is an estimate of a source. The challenge lies in finding the ICs. In DSP, all received inputs are sampled at the same time. The joint distribution of these samples is sufficient to recover the ICs. In the analog case, one could imagine scanning through the received signals and storing their waveforms, as in [20]–[22]; however, waveform content changes upon each successive measurement. Since multivariate samples are not synchronized, the joint distribution cannot be observed.
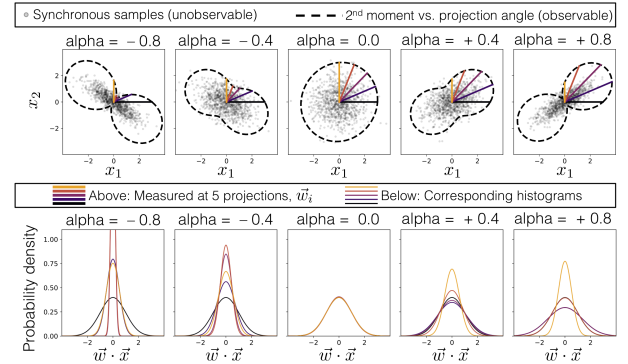
Instead of attempting to recover waveforms, our approach uses measurements of univariate statistical properties described by moments: the expectation value or time-average of the variable raised to a power. The bth moment of the output is denoted as $\langle m^b \rangle_t$, where $\langle \cdot \rangle_t$ is a time average. Moments are time-invariant when the channel mixing is stationary. In an RF context, stationary times are on timescales related to environmental and channel fluctuations, which are orders of magnitude slower than the signals themselves. Since no attempt to reconstruct signal waveforms is required, the additional sampling needed to measure moments can be deeply below the Nyquist rate.

The 2nd-order moment can be parameterized by weight vector angle using unit normal weight vectors. In this case, the moment vs. angle relationship follows a model of the form:

$$\vec{w}(\theta) = [\cos\theta, \sin\theta] \tag{2}$$
$$\langle m^2 \rangle_t (\theta) = q_1 + q_2 \cos[2(\theta - \theta_0)] \tag{3}$$

where q_1, q_2, and θ_0 are time-invariant parameters. Eq. (3), referred to as a two-petal epitrochoid, has a clear relation to the principal components. The magnitude of the first component is $q_1 + q_2$, and that of the second is $q_1 - q_2$. The first PC vector angle is θ_0, and the second is orthogonal. The q and θ parameters describe *all* of the covariance properties of the joint distribution.

This model in polar coordinates is shown in Fig. 2 over a range of correlation values, alpha. As the correlation between x_1 and x_2 increases, the distribution becomes more stretched and narrow, and the angular moment model begins to show two petals. The relationship between the joint sample distribution and the epitrochoid are clear; however, the joint samples require simultaneous measurement of all channels. Given our constraints, the joint samples are unobservable, while the epitrochoid is observable.

B. Successive Moment Fitting Algorithm

The algorithm proceeds by reconfiguring an analog weight bank to project the inputs onto a chosen succession of projection angles and then measuring the projection moment. These measurements are represented in Fig. 2 (top) as colored vectors. For different correlation parameters, the histogram of the projected signal (bottom) changes in different ways vs. projection angle. These variance measurements can be fit with the model of Eq. (3) by breaking the fitting problem down into a linear pseudo-inverse problem and a convex nonlinear optimization problem. For multiple measurements, Eq. (3) becomes a linear system of the form

$$\begin{bmatrix} \langle m^2 \rangle_t (\theta_1) \\ \cdots \\ \langle m^2 \rangle_t (\theta_K) \end{bmatrix} = \begin{bmatrix} 1 & \cos\left[2(\theta_1 - \theta_0)\right] \\ \cdots & \cdots \\ 1 & \cos\left[2(\theta_K - \theta_0)\right] \end{bmatrix} \cdot \begin{bmatrix} q_1 \\ q_2 \end{bmatrix} \quad (4)$$

where K is the number of measurements. A guess of θ_0 is posited, and then the q vector can be found quickly using the pseudo-inverse, resulting in a fitting error. The Gauss/Legendre pseudo-inverse is used for an efficient solution for fitting noisy measurements with optimal error in systems of this formulation. The fitting error is mimized over θ_0 using gradient descent, straightforward in this case because the model is convex in θ_0 and θ_0 bounded on the $[0, \pi)$ interval.

Normalizing the principal components results in a new set of *whitened* signals, whose variance is equal over all projection angles in the whitened basis. The whitening process is mathematically described by a scaling transform: $\mathbf{U\Sigma U}^{-1}$, where $\mathbf{U}$ is a rotation matrix by angle θ_0, and $\mathbf{\Sigma}$ is a diagonal scaling matrix whose first element is 1 and last element is $(q_1 + q_2)/(q_1 - q_2)$.

After whitening, the independent components are identified using a similar moment fitting method. We parameterize by a new angle, ϕ, in the whitened basis. The 4th-order moments then take the form of a 4-petal epitrochoid.

$$\vec{w} = \mathbf{U\Sigma U}^{-1} \left[\cos\phi, \sin\phi\right] \quad (5)$$
$$\langle m^4 \rangle_t (\phi) = p_1 + p_2 \cos\left[2(\phi - \phi_0)\right] \quad (6)$$
$$\ldots + p_3 \cos\left[4(\phi - \phi_0)\right] \quad (7)$$

ϕ_0 is determined by the Gauss/Legendre and gradient descent method described above. Finally, the transformations are composed as $\hat{A}^{-1}$ whose row vectors are the weights that demix the source signals.

$$\hat{\mathbf{A}}^{-1} = \mathbf{VU\Sigma U}^{-1} = \begin{bmatrix} \vec{w}_{IC,1} \\ \vec{w}_{IC,2} \end{bmatrix} \quad (8)$$

The successive moment fitting algorithm is verified though simulation in Fig. 3. In each case, the sources occupy the same frequency bands, so they cannot be filtered. The columns represent the steps of the algorithm: (i) received basis, (ii) whitened basis, (iii) separated basis. The 4 element mixing matrices are chosen randomly. In (i), the orange curve are observable measurements of the variance vs. projection angle: $\langle m^2 \rangle_t (\theta)$. Each row represents a different type of kurtosis in the signals. Gaussian distributions have a kurtosis of 3, shown as a black dashed circle and used as a baseline. Uniform distributions are sub-Gaussian, meaning they have kurtosis
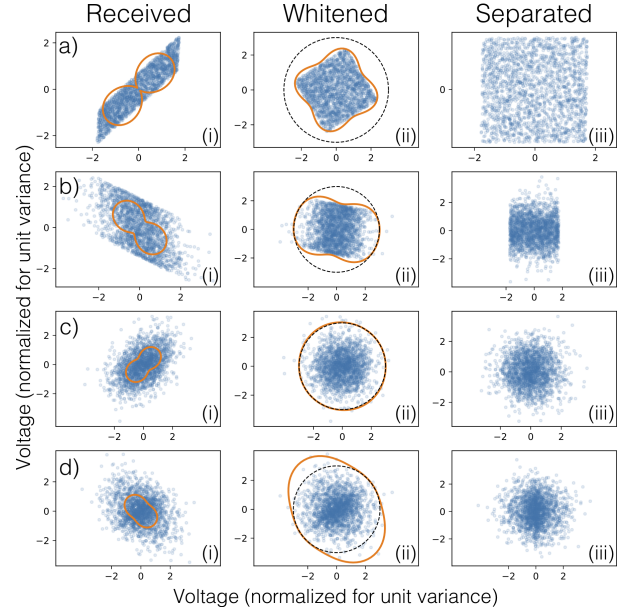

Fig. 3. Simulations of the successive moment fitting algorithm with different source statistics. Row a) uniform/uniform; Row b) uniform/Gaussian; Row c) Gaussian/Gaussian is not separable; Row d) AM/Gaussian. In (i-iii), blue dots: synchronous samples (unobservable) for reference. Column (i) are the signals received at the antennas. Orange curve: 2nd-order moments (variance) vs. projection angle. Column (ii) are the same signals plotted in the whitening basis. Orange curve: 4th-order moments (kurtosis) vs. projection angle. Black dashed circle: Gaussian kurtosis of 3. Column (iii) are the signals in the independent component basis. In this basis, projecting along the x or y axes gives the estimates of the original sources.

less than 3. The distribution of an amplitude modulated (AM) signal is super-Gaussian. In (ii), the orange curves are fourth-order moment measurements made in the transformed basis: $\langle m^4 \rangle_t (\phi)$. In (iii), the distributions appear orthonormal, indicating success of the algorithm. Each signal can be recovered by projecting along $[0, 1]$ or $[1, 0]$ in this basis.

III. DEMONSTRATION

To demonstrate proof-of-concept, we use RF photonic weighted addition setup, although results also apply to RF electronic weighted addition. RF photonics has attracted recent interest because it can provide advantages to bandwidth, dynamic range, tunability, and power use. In an RF photonic processor, incoming signals are modulated onto an optical carrier wave, processed in some way, detected, and, only then, digitized. Integrated RF photonics has offered performance improvements for programmable filtering [23], [24], time delays [25], [26], and waveform generation [27], [28]. Photonic weighted addition is implemented using power-modulated, mutually incoherent optical carriers impinging on a photodetector. Microring (MRR) weight banks [29] bring photonic weighted addition to silicon photonics. They are capable of applying weights that are balanced [30], continuous [31], and independent [32].

A. Methods

We fabricate silicon waveguides (WGs) with 220nm thickness and 500nm width on top of a buried oxide layer.
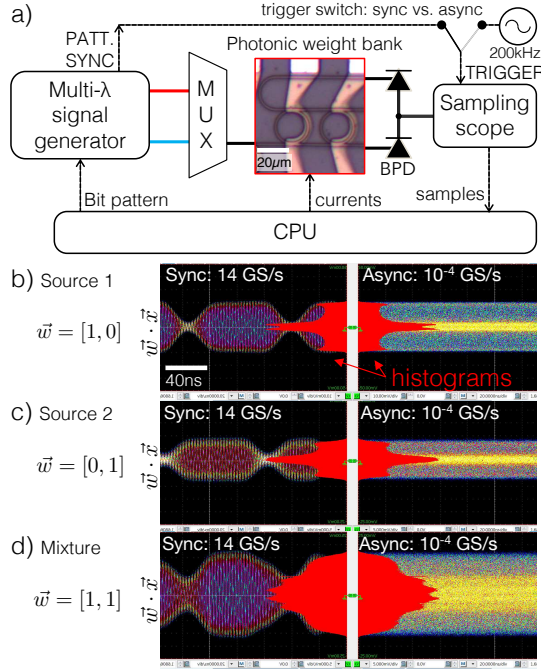
Fig. 4. Demonstration of recovering univariate statistics while obscuring waveforms using photonic hardware. a) Experimental setup showing signal generation, WDM weighting, and measurement (Oscope). Each subsystem is controlled by computer (CPU). The Oscope is triggered by either the pattern sync (PATT. SYNC) of the signal generator or by a free-running clock. b-d) Oscope views over both synchronization states. The effective sample rate is super-Nyquist in the sync state (left column) and deeply sub-Nyquist in the async state (right column). Signal histograms (red) are identical even though waveform information is lost. Three weight vectors are chosen to obtain source 1 (b), source 2 (c), and a mixture (d).

Ti/Au tuning contacts were then deposited on top of an oxide passivation layer. The device consists of two bus waveguides and two MRRs in a parallel add/drop configuration, each with a thermal tuning element (Fig. 4a). Fibers are coupled to chip using focusing subwavelength grating couplers [33]. The multi-wavelength (multi-λ) signal generator modulates a single RF waveform onto two wavelengths with a relative delay offset of 60ns. Modulating waveforms have 900MHz center frequency with bitrate of 50 Mbps (limited by instruments). The signal generator produces a pattern synchronization (PATT. SYNC) trigger that is time-locked to the waveform, which repeats every 2.56μs (10^7 bit periods). These outputs are wavelength division multiplexed (WDM/MUX) and sent to the MRR weight bank. A computer (CPU) controls the signal pattern and applied photonic weights, also observing the samples taken by the Oscope.

B. Constraining observability

We introduce an experimental method for emulating blindness, constraining what can be observed to correspond to a realistic scenario. In a field (i.e. real life) scenario, waveforms are non-periodic. The only way to obtain an accurate digital waveform is to take samples in a real-time order at a real-time rate greater than the Nyquist frequency. In a laboratory setting, periodic waveforms are often used so that samples can be taken over multiple periods at different phases of the repeating waveform. In this way, a "sampling scope" can synthesize a digital waveform equivalent to that which would be obtained by a much faster "real-time scope." We refer to that rate as the synthetic sampling rate.

Examples of not sufficiently realistic strategies are found in past work on RF photonic PCA with fiber components [20]–[22]. To ascertain the original inputs, these works scanned through identity projections of the form $[1, 0, 0, \ldots]$, thereby making the unrealistic assumption that inputs are synchronized and repeating with a period known precisely to the receiver performing PCA.

To experimentally evaluate a blind source separation algorithm, the input and converged signals of course must be observed. At the same time however, we must ensure that the artificial synchronization between signal generator and sampling scope is not exploited by the algorithm. We accomplish these goals on the hardware level by toggling the triggering state of a sampling oscilliscope, a Tektronix DSA8300. The trigger switching setup is shown in the diagram in Fig. 4a. In the synchronous state, the pattern sync output triggers the scope, allowing it to emulate a super-Nyquist real-time ADC (here 14GS/s). In the asynchronous state, a free running clock triggers the scope, creating a situation equivalent to deeply sub-Nyquist real-time ADC (here, 2×10^{-4}GS/s). In the asynchronous state, the scope loses the ability to synthesize an accurate digital waveform.

C. Results

Fig. 4 illustrates the difference in observability caused by the trigger switching. In moving from synchronous to asynchronous sampling, waveform information is lost, but voltage histograms (red) are maintained. This illustrates that deeply sub-Nyquist, asynchronous sampling provides sufficient statistical information for successive subspace moment algorithms. The observability of stationary statistics but not waveforms enforces a correspondence between the laboratory and field scenarios on a hardware level. In the third row, a weight vector is applied to represent a mixture of the two inputs. We observe that the mixtures of two independent test signals is more Gaussian than either constituent, and that this is observable without waveform knowledge.

IV. APPLICATION TO PRIVACY IN SPECTRUM MONITORING

Cognitive radio or opportunistic spectrum sharing promises to radically increase dynamic spectral efficiency in distributed, non-cooperative environments [34]. Opportunistic access requires advanced hardware and signal processing techniques that are more likely to malfunction or fail to meet compliance by disrupting the operation of other users [35]. Spectrum monitoring, analysis, and enforcement operations will become an indispensable safeguard against a chaotic descent into a new "tragedy of the commons" [36]. At the same time, spectrum monitoring represents a privacy threat to compliant users [37]. The physical layer provides a strong protection against the incessant cyber threats permeating the digital domain.

A common goal of spectrum monitoring operations is to detect the presence of non-compliance that interferes with
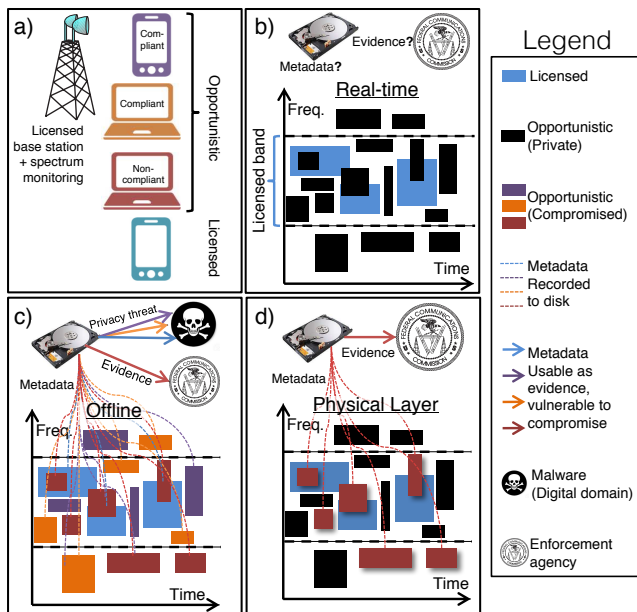
Fig. 5. A spectrum monitoring scenario (a) where source separation analysis is attempted in real-time (b), offline (c), or in the physical layer (d). The goal is to get the metadata of the non-compliant user (red) to an enforcement agency without compromising that of the licensed (blue) and compliant (purple, organge) users.

priority spectrum access, such as that between a licensed cellular base station and customer. An example scenario is depicted in Fig. 5a, which includes a licensed user (blue), two compliant opportunistic users (orange, purple), and one non-compliant opportunistic user (red). Fig. 5b-c represent the time-resolved spectrum as seen at the base station. Detection alone does not provide a mitigation solution. Some form of actionable evidence must be gathered to prove the non-compliance of the identified transmitter, thereby providing justification for enforcement actions.

Monitoring opportunistic users is challenging due to the unpredictability and transience of time-frequency transmission blocks, compounded with the presence of multiple simultaneous transmitters [38]. Simply recording the entire spectrum can detect but not identify sources of interference. This case of failure to identify is illustrated in Fig. 5b. Attributing transmission blocks to individual users requires advanced analysis that cannot be performed in real-time. Instead, this analysis can be performed offline after recording all spectral data. The offline approach introduces a serious privacy risk to the content and/or metadata of *all* users [39]. This situation of failure to protect is pictured in Fig. 5c. As soon as information is recorded to disk, its security is considered compromised [40]–[42]. Even if the monitoring operator is considered benign, it may be unknowingly harboring malware that can then access the content of all spectrum users [43].

BSS in the physical layer can preserve widespread privacy by isolating non-compliant transmissions in the analog domain, thereby preventing compliant user signals from reaching the disk, as shown in Fig. 5c. The privacy of compliant users (orange and purple) is strongly preserved,

while the monitoring operation can gather sufficient evidence on the non-compliant user (red). The privacy threat to the non-compliant user should be considered acceptable because it is the minimum application-specific information required to complete the enforcement task.

V. DISCUSSION

Further work on the algorithm could include studies of convergence and extension to arbitrary dimensions. It is expected that there will be some threshold of signal-to-noise ratio at which point the algorithm fails to converge. The concept of physical layer BSS could extend to more dimensions. Separating mixtures of N channels would require N antennas, at least N measurements, and an N dimensional generalization of the model. An important question will be how to efficiently perform optimization of the nonlinear parts of the fitting algorithm. Above, we found this optimization to be convex and bounded. It is probable that gradient descent will still succeed in higher dimensions.

This paper calls for further work in experimental demonstration. For experimental PCA, a signal generator capable of producing correlated signals will be needed, as well as a weight bank that can set weights accurately given desired projection angles. For experimental ICA, the generated signals must come from independent sources and then mixed in a hardware mixing network or channel emulator. Furthermore, the various algorithm enhancements discussed above should be experimentally studied.

VI. CONCLUSION

While offering transformative performance characteristics, the analog multi-input front-end introduces a barrier to finding the weight vectors of interest. We introduced a novel compatible algorithm for using univariate subspace statistics to reconstruct the multivariate statistical properties required for PCA, ICA, and BSS. This approach makes minimal a priori assumptions about the source signals and could be extended to more complex scenarios. We also demonstrated a method for emulating realistic receiver blindness in experiment, indispensible in further experimental work in this area. Blind source separation is widely applicable to RF scenarios where source signals are mixed over the air. As an example, we outlined an application in spectrum monitoring in which compliant user metadata is protected in the physical layer. BSS in the physical layer offers substantial advantages for performance and new techniques for preserving privacy in multi-antenna systems.

REFERENCES

[1] E. Dahlman, G. Mildh, S. Parkvall, J. Peisa, J. Sachs, Y. Selén, and J. Sköld, "5G wireless access: requirements and realization," *IEEE Communications Magazine*, vol. 52, no. 12, pp. 42–47, December 2014.

[2] A. Osseiran, F. Boccardi, V. Braun, K. Kusume, P. Marsch, M. Maternia, O. Queseth, M. Schellmann, H. Schotten, H. Taoka, H. Tullberg, M. A. Uusitalo, B. Timus, and M. Fallgren, "Scenarios for 5g mobile and wireless communications: the vision of the metis project," *IEEE Communications Magazine*, vol. 52, no. 5, pp. 26–35, May 2014.

[3] E. Biglieri, R. Calderbank, A. Constantinides, A. Goldsmith, A. Paulraj, and H. V. Poor, *MIMO wireless communications*. Cambridge University Press, 2007.

[4] A. Hyvärinen and E. Oja, "Independent component analysis: Algorithms and applications," *Neural Networks*, vol. 13, no. 4-5, pp. 411–430, 2000.

[5] J.-F. Cardoso and A. Souloumiac, "Blind beamforming for non gaussian signals," *IEE Proceedings-F*, vol. 140, pp. 362–370, 1993.

[6] R. H. Lambert and A. J. Bell, "Blind separation of multiple speakers in a multipath environment," in *1997 IEEE International Conference on Acoustics, Speech, and Signal Processing*, vol. 1, 1997, pp. 423–426 vol.1.

[7] R. H. Walden, "Analog-to-digital converter survey and analysis," *IEEE Journal on Selected Areas in Communications*, vol. 17, no. 4, pp. 539–550, Apr 1999.

[8] B. Murmann, "The race for the extra decibel: A brief review of current adc performance trajectories," *IEEE Solid-State Circuits Magazine*, vol. 7, no. 3, pp. 58–66, Summer 2015.

[9] V. Venkateswaran and A. J. van der Veen, "Analog beamforming in mimo communications with phase shift networks and online channel estimation," *IEEE Transactions on Signal Processing*, vol. 58, no. 8, pp. 4131–4143, Aug 2010.

[10] F. Gholam, J. Via, and I. Santamaria, "Beamforming design for simplified analog antenna combining architectures," *IEEE Transactions on Vehicular Technology*, vol. 60, no. 5, pp. 2373–2378, Jun 2011.

[11] S. Han, C. l. I, Z. Xu, and C. Rowell, "Large-scale antenna systems with hybrid analog and digital beamforming for millimeter wave 5g," *IEEE Communications Magazine*, vol. 53, no. 1, pp. 186–194, January 2015.

[12] S. Kutty and D. Sen, "Beamforming for millimeter wave communications: An inclusive survey," *IEEE Communications Surveys Tutorials*, vol. 18, no. 2, pp. 949–973, Secondquarter 2016.

[13] S.-Y. Lee, S. Choi, A. Cichocki, and H.-M. Park, "Blind source separation and independent component analysis: A review," *Neural Information Processing - Letters and Reviews*, vol. 6, no. 1, pp. 1–57, 2005.

[14] H. Ghauch, T. Kim, M. Bengtsson, and M. Skoglund, "Subspace estimation and decomposition for large millimeter-wave MIMO systems," *IEEE Journal of Selected Topics in Signal Processing*, vol. 10, no. 3, pp. 528–542, April 2016.

[15] A. Alkhateeb, O. E. Ayach, G. Leus, and R. W. Heath, "Channel estimation and hybrid precoding for millimeter wave cellular systems," *IEEE Journal of Selected Topics in Signal Processing*, vol. 8, no. 5, pp. 831–846, Oct 2014.

[16] K. Venugopal, A. Alkhateeb, N. G. Prelcic, and R. W. Heath, "Channel estimation for hybrid architecture-based wideband millimeter wave systems," *IEEE Journal on Selected Areas in Communications*, vol. 35, no. 9, pp. 1996–2009, Sept 2017.

[17] N. B. Zanjani, S. Khademi, and G. Leus, "Gradient-based solution for hybrid precoding in mimo systems," in *2017 IEEE International Conference on Acoustics, Speech and Signal Processing (ICASSP)*, March 2017, pp. 3489–3493.

[18] T. Dahl, N. Christophersen, and D. Gesbert, "Blind mimo eigenmode transmission based on the algebraic power method," *IEEE Transactions on Signal Processing*, vol. 52, no. 9, pp. 2424–2431, Sept 2004.

[19] R. A. Iltis, S.-J. Kim, and D. A. Hoang, "Noncooperative iterative mmse beamforming algorithms for ad hoc networks," *IEEE Transactions on Communications*, vol. 54, no. 4, pp. 748–759, April 2006.

[20] A. N. Tait, J. Chang, B. J. Shastri, M. A. Nahmias, and P. R. Prucnal, "Demonstration of WDM weighted addition for principal component analysis," *Opt. Express*, vol. 23, no. 10, pp. 12 758–12 765, May 2015.

[21] T. Ferreira de Lima, A. N. Tait, M. A. Nahmias, B. J. Shastri, and P. R. Prucnal, "Scalable wideband principal component analysis via microwave photonics," *IEEE Photonics Journal*, vol. 8, no. 2, pp. 1–9, April 2016.

[22] A. N. Tait, T. F. de Lima, E. Zhou, A. X. Wu, M. Chang, M. A. Nahmias, B. J. Shastri, and P. R. Prucnal, "Silicon microring weight banks for

multivariate rf photonics," in *Conference on Lasers and Electro-Optics*. Optical Society of America, 2017, p. SM1O.6.

[23] D. Pérez, I. Gasulla, L. Crudgington, D. J. Thomson, A. Z. Khokhar, K. Li, W. Cao, G. Z. Mashanovich, and J. Capmany, "Multipurpose silicon photonics signal processor core," *Nature Communications*, vol. 8, no. 1, p. 636, 2017.

[24] L. Zhuang, C. G. H. Roeloffzen, M. Hoekman, K.-J. Boller, and A. J. Lowery, "Programmable photonic signal processor chip for radiofrequency applications," *Optica*, vol. 2, no. 10, pp. 854–859, Oct 2015.

[25] Y. Liu, A. Choudhary, D. Marpaung, and B. J. Eggleton, "Gigahertz optical tuning of an on-chip radio frequency photonic delay line," *Optica*, vol. 4, no. 4, pp. 418–423, Apr 2017.

[26] M. Burla, L. R. Cortés, M. Li, X. Wang, L. Chrostowski, and J. A. na, "Integrated waveguide bragg gratings for microwave photonics signal processing," *Opt. Express*, vol. 21, no. 21, pp. 25 120–25 147, Oct 2013.

[27] M. H. Khan, H. Shen, Y. Xuan, L. Zhao, S. Xiao, D. E. Leaird, A. M. Weiner, and M. Qi, "Ultrabroad-bandwidth arbitrary radiofrequency waveform generation with a silicon photonic chip-based spectral shaper," *Nature: Photonics*, vol. 4, no. 2, pp. 117–122, Feb 2010.

[28] A. M. Weiner, "Ultrafast optical pulse shaping: A tutorial review," *Optics Communications*, vol. 284, no. 15, pp. 3669 – 3692, 2011, special Issue on Optical Pulse Shaping, Arbitrary Waveform Generation, and Pulse Characterization.

[29] A. N. Tait, A. X. Wu, T. Ferreira de Lima, E. Zhou, B. J. Shastri, M. A. Nahmias, and P. R. Prucnal, "Microring weight banks," *IEEE J. Sel. Top. Quantum Electron.*, vol. 22, no. 6, 2016.

[30] A. N. Tait, M. A. Nahmias, B. J. Shastri, and P. R. Prucnal, "Broadcast and weight: An integrated network for scalable photonic spike processing," *J. Lightwave Technol.*, vol. 32, no. 21, pp. 4029–4041, Nov 2014.

[31] A. Tait, T. Ferreira de Lima, M. Nahmias, B. Shastri, and P. Prucnal, "Continuous calibration of microring weights for analog optical networks," *Photonics Technol. Lett.*, vol. 28, no. 8, pp. 887–890, April 2016.

[32] A. N. Tait, T. Ferreira de Lima, M. A. Nahmias, B. J. Shastri, and P. R. Prucnal, "Multi-channel control for microring weight banks," *Opt. Express*, vol. 24, no. 8, pp. 8895–8906, Apr 2016.

[33] Y. Wang, X. Wang, J. Flueckiger, H. Yun, W. Shi, R. Bojko, N. A. Jaeger, and L. Chrostowski, "Focusing sub-wavelength grating couplers with low back reflections for rapid prototyping of silicon photonic circuits," *Opt. Express*, vol. 22, no. 17, pp. 20 652–20 662, 2014.

[34] I. F. Akyildiz, W. y. Lee, M. C. Vuran, and S. Mohanty, "A survey on spectrum management in cognitive radio networks," *IEEE Communications Magazine*, vol. 46, no. 4, pp. 40–48, April 2008.

[35] R. Chen, J. m. Park, Y. T. Hou, and J. H. Reed, "Toward secure distributed spectrum sensing in cognitive radio networks," *IEEE Communications Magazine*, vol. 46, no. 4, pp. 50–55, April 2008.

[36] G. Faulhaber and D. Farber, "Spectrum management: Property rights, markets and the commons," in *Proc. of the Telecommunications Policy Research Conference*, 2003.

[37] A. G. Fragkiadakis, E. Z. Tragos, and I. G. Askoxylakis, "A survey on security threats and detection techniques in cognitive radio networks," *IEEE Communications Surveys Tutorials*, vol. 15, no. 1, pp. 428–445, First 2013.

[38] J. L. Burbank, "Security in cognitive radio networks: The required evolution in approaches to wireless network security," in *2008 3rd International Conference on Cognitive Radio Oriented Wireless Networks and Communications (CrownCom 2008)*, May 2008, pp. 1–7.

[39] T. C. Clancy and N. Goergen, "Security in cognitive radio networks: Threats and mitigation," in *2008 3rd International Conference on Cognitive Radio Oriented Wireless Networks and Communications (CrownCom 2008)*, May 2008, pp. 1–8.

[40] A. Evfimievski, J. Gehrke, and R. Srikant, "Limiting privacy breaches in privacy preserving data mining," in *Proceedings of the Twenty-second ACM SIGMOD-SIGACT-SIGART Symposium on Principles of Database Systems*, ser. PODS '03. New York, NY, USA: ACM, 2003, pp. 211–222.

[41] A. Acquisti, A. Friedman, and R. Telang, "Is there a cost to privacy breaches: An event study," in *ICIS Proceedings*, 2006.

[42] J. O. Christensen, "Wrong on red: The constitutional case against red-light cameras note," *Washington University Journal of Law and Policy*, p. 443, 2010.

[43] S. Romanosky, A. Acquisti, and R. Sharp, "Data breaches and identity theft: When is mandatory disclosure optimal?" in *TPRC*, 2010.